The Structure of the Membrane Distal Phosphatase Domain of RPTPα Reveals Interdomain Flexibility and an SH2 Domain Interaction Region†

Erica Dutil Sonnenburg,‡ Alexandrine Bilwes,‡,§ Tony Hunter,|| and Joseph P. Noel*,‡

Structural Biology Laboratory and Molecular and Cell Biology Laboratory, The Salk Institute for Biological Studies, 10010 North Torrey Pines Road, La Jolla, California 92037

Received January 13, 2003; Revised Manuscript Received April 28, 2003

ABSTRACT: The receptor protein tyrosine phosphatase α (RPTPα) is a transmembrane receptor with two intracellular protein tyrosine phosphatase domains, a catalytically active membrane proximal domain (D1) and a membrane distal phosphatase domain with minimal catalytic activity (D2). Here we elucidate the crystal structure of RPTPα's D2 domain. Unlike D1, D2 exists as a monomer and lacks the N-terminal inhibitory wedge motif. The N-terminal portion of D2 is disordered, and this region linking D1 to D2 is proteolytically labile in solution whether part of D2 alone or tethered to D1, indicating that the polypeptide backbone of this part of D2 is highly flexible, and therefore accessible to proteases under native conditions. Furthermore, we have crystallized the SH2 domain of the protein tyrosine kinase c-Src, a RPTPα substrate, with a phosphopeptide encompassing the C-terminal phosphorylation site of D2 (pTyr789). The SH2 domain of Src binds RPTPα in an extended conformation. The structural and functional data support a D1−D2 arrangement with significant flexibility between phosphatase domains of RPTPα that is likely to be important for dynamic alterations in intra- and/or intermolecular interactions that are critical for RPTPα function.

The receptor protein tyrosine phosphatases (RPTPs)[1] are a family of transmembrane phosphatases responsible for the hydrolysis of the phosphate moiety from a pTyr residue in target phosphoprotein substrates resulting in a variety of intracellular responses, including long-term potentiation, axonal path finding and neural transmission, and transformation (reviewed in refs *1* and *2*). The RPTPs consist of an extracellular domain, a single spanning transmembrane region, and two tandem intracellular tyrosine phosphatase domains, with the exception of a small subgroup of RPTPs that contain a single phosphatase domain. The majority of diversity within the RPTP family lies within the extracellular domain and includes protein modules such as immunoglobin-like domains, fibronectin type III-like domains, and heavily glycosylated polypeptide segments. In contrast, the sequences and structures of intracellular tyrosine phosphatase domains are highly homologous not only within the RPTP family but also with those of the nonreceptor tyrosine phosphatases (reviewed in refs *3* and *4*).

The first, membrane proximal, phosphatase domain, D1, harbors most, or in some cases, all of the catalytic activity. All active tyrosine phosphatases contain an active site cysteine, which forms a cysteinyl phosphate intermediate following nucleophilic attack on the pTyr substrate, as well as a conserved Asp that acts as a general acid−base catalyst to complete the water-mediated hydrolysis of the cysteinyl phosphate intermediate. The membrane distal phosphatase domain, D2, a highly conserved domain within the RPTP family, exhibits little or no phosphatase activity despite the fact that it possesses the catalytic cysteine residue required for nucleophilic attack and a conservative substitution, Glu, in place of the general acid−base Asp catalytic residue.

Two independent crystal structures of the membrane proximal phosphatase domain, D1, of RPTPα reveal a crystallographic dimer arrangement in which the active site of one domain is occluded by a helix−turn−helix wedge motif of its dyad related partner (*5*). The use of engineered disulfide bonds in full-length RPTPα demonstrates that this dimeric configuration renders RPTPα catalytically inactive *in vivo* (*6*). Since the initially determined RPTPα D1 crystal structure, a plethora of evidence supporting dimerization as an important regulatory mechanism in some RPTPs has surfaced. The most compelling evidence for RPTPα dimerization is the observation of fluorescence resonance energy transfer (FRET) between cyan and yellow derivatives of the green fluorescent protein fused to RPTPα *in vivo*. Truncations of RPTPα reveal that the transmembrane region is necessary and sufficient for dimerization as measured by FRET and chemical cross-linking (*7*, *8*). Therefore, the D1

† This work was supported by NIH/NCI Grant CA54418 to J.P.N. and T.H. and a postdoctoral training grant (T32CA09370) to E.D.S. T.H. is a Frank and Else Schilling American Cancer Society Research Professor. The SSRL Biotechnology Program is supported by the National Institutes of Health, National Center for Research Resources, Biomedical Technology Program, and by the Department of Energy, Office of Biological and Environmental Research.

* To whom correspondence should by addressed. Telephone: (858) 453-4100. Fax: (858) 452-3683. E-mail: noel@salk.edu.

‡ Structural Biology Laboratory.

§ Present address: Department of Chemistry and Chemical Biology, Cornell University, G-60 ST Olin, Ithaca, NY 14853.

|| Molecular and Cell Biology Laboratory.

[1] Abbreviations: RPTP, receptor protein tyrosine phosphatase; PMSF, phenylmethanesulfonyl fluoride; DTT, dithiothreitol; PEG, polyethylene glycol; SDS, sodium dodecyl sulfate; PAGE, polyacrylamide gel electrophoresis; PVDF, polyvinylidene difluoride; pTyr, phosphotyrosine; rmsd, root-mean-square deviation.

10.1021/bi0340503 CCC: $25.00
Published on Web 06/11/2003

domain wedge motif may only serve to stabilize RPTPα's dimeric state and occlude the related D1's active site, whereas the transmembrane region most likely provides the energetic driving force for dimerization. Evidence that dimerization plays a key role in the negative regulation of another RPTP family member, CD45, has emerged. Specifically, a transgenic mouse expressing CD45 with a point mutation that should disrupt inhibition via active site occlusion involving the inhibitory wedge motif results in a phenotype consistent with CD45 activation (*9*, *10*). However, dimerization may not be a universal regulatory mechanism employed by all RPTPs. The crystal structures of the D1 phosphatase domain of RPTPμ and the D1D2 phosphatase domains of LAR do not show occluded dimer architectures despite the fact that each contains an intact wedge motif (*11*, *12*).

A functional role for the D2 domain is much less clear than for the D1 domain, since the D2 domain displays little or no catalytic activity but is highly conserved across a diverse set of RPTPs. Recent evidence suggests that the D2 domain may be important for regulating D1 phosphatase activity through intra- or intermolecular interactions. An intramolecular interaction between D2 and D1 was demonstrated for CD45, as well as between D2 and the region N-terminal to D1 (juxtamembrane region) in RPTPμ (*13*, *14*). For RPTPα, a reversible intramolecular interaction in response to oxidative stress was described between the spacer region (the region connecting the D1 and D2 domains) and the C-terminus that is dependent on the catalytic cysteine of the D2 domain (*15*). The catalytic cysteine of D2 is also required for a peroxide-induced conformational change in the extracellular domain of RPTPα *in vivo*, implicating the D2 domain in RPTPα extracellular signaling (*16*).

Yeast two-hybrid screens and co-immunoprecipitation studies have identified a variety of intermolecular interactions between D2 domains and the wedge region of D1 domains from heterologous RPTP family members (*17*−*19*). Furthermore, RPTPα−LAR heterodimers were observed *in vivo* (*19*). Heterodimer formation in a combinatorial fashion may allow for an increase in the diversity of downstream signaling pathways encompassing RPTPs. Alternatively, the formation of mixed D2−D1 heterodimers could initiate RPTP activity by disrupting wedge-mediated D1 dimer formation.

Moreover, D2 domains may function during the selection of proteins targeted for dephosphorylation by the catalytically active D1 domain. For CD45, the ability to co-immunoprecipitate the substrate TCR-ζ requires its D2 domain, since replacement of CD45's D2 domain with the D2 domain of LAR abolishes the CD45−TCR-ζ association (*20*). Another example of a D2 domain being critical in substrate selection involves RPTPα. *In vivo*, approximately 20% of the RPTPα population is phosphorylated on Tyr789, a conserved residue lying very close to the C-terminus of many RPTPs. For RPTPα, this pTyr residue serves as a docking site for the SH2 domain containing adaptor protein Grb2 (*21*). Recently, the tyrosine kinase c-Src, an RPTPα substrate, has also been shown to interact with RPTPα's D2 C-terminal Tyr789 via Src's SH2 domain. Src SH2 binding to RPTPα results in dephosphorylation of c-Src's inhibitory phosphorylation site (Tyr527), leading to c-Src activation (*22*). In a more recent study, Zheng et al. (*23*) describe a model in which the C-terminus of RPTPα is bound to Grb2 under resting conditions; however, upon phosphorylation at Ser180 and/or Ser204 of RPTPα, Src's SH2 domain displaces Grb2, leading to dephosphorylation of c-Src by RPTPα. *In vivo*, RPTPα is known to be phosphorylated at Ser180 and Ser204 by protein kinase C, the stoichiometry of which is increased upon stimulation of cells with the protein kinase C activator, phorbol ester (*24*). Zheng et al. hypothesize that phosphorylation of Ser180 and/or Ser204 in the juxtamembrane region stabilizes the interaction with the C-terminus, causing it to adopt an extended conformation. This extended conformation would then favor Src SH2 binding over Grb2 SH2 binding, since the latter prefers to bind pTyr in a β-turn configuration (*23*).

In this paper, we investigate the functional role of the membrane distal phosphatase domain (D2) of RPTPα by determining the crystal structure of the D2 domain as well as the structure of a phosphopeptide designed to mimic RPTPα's C-terminus bound to the SH2 domain of chicken c-Src. The D2 domain, unlike D1, does not possess an inhibitory wedge, nor is it sufficient for dimer formation. However, the structure determination of D2 reveals that the N-terminal region of D2 is highly flexible. Limited proteolysis of the D1D2 protein confirms the presence of a flexible D2 N-terminal region. D2 flexibility may be important in allowing formation of intra- or intermolecular interactions between the D2 domain and the D1 or juxtamembrane serine phosphorylation sites, as has been reported. Furthermore, D1's ability to dephosphorylate substrates bound to the D2 domain, such as Src, may again be dependent on D1−D2 interdomain flexibility.

MATERIALS AND METHODS

Materials. The pET-28a(+) expression vector and *Escherichia coli* strain BL21(DE3) were obtained from Novagen (Madison, WI). The pHIS8 expression vector was assembled as described previously (*25*). The QuikChange polymerase chain reaction (PCR)-based site-directed mutagenesis kit was from Stratagene (La Jolla, CA). All oligonucleotides were ordered from Operon (Alameda, CA). Restriction enzymes, T4 ligase, dNTPs, and Vent polymerase were obtained from New England Biolabs (Beverly, MA). Ni^{2+}−NTA resin was purchased from Qiagen (Valencia, CA). Benzamidine-Sepharose and the Superdex-200 FPLC column were from Amersham Biosciences (Piscataway, NJ). Thrombin was obtained from Sigma (St. Louis, MO). All peptides were synthesized and purchased from SynPep Corp. (Dublin, CA).

Construction of Expression Vectors. Murine RPTPα D2 (residues Ile512−Ser787) was amplified by PCR using 5′-TGCCGCGCGGCAGC**CATATG**ATTTATAACAAGATCCCA as the forward primer and 5′-CGACGGAGCTCGAATTC**GGATCC**TTATGAAAAGGCGTCAATGT as the reverse primer. The PCR product was digested with *Nde*I and *Bam*HI (recognition sites in bold), gel purified, and ligated into *Nde*I- and *Bam*HI-digested pET-28a(+). A truncated version of the murine RPTPα D1D2 sequence (Lys208−Ser787) was amplified from a full-length cDNA by PCR using 5′-TGCCGCGCGGCAGC**CATATG**AAGTACCCACCACTGCCT as the forward primer and 5′-CGACGGAGCTCGAATTC**GGATCC**TTATGAAAAGGCGTCAATGT as the reverse primer. The PCR product was digested with *Nde*I and *Bam*HI (cleavage sites highlighted above), gel purified, and ligated into *Nde*I- and *Bam*HI-

digested pET-28a(+). The chicken c-Src SH2 domain (residues Ala158−Pro259) was amplified by PCR from an expression plasmid using 5′-dCATG**CCATGG**CCAGGCTGAAGAGTGGTAC as the forward primer and 5′-CGC**GGATCC**CTACTTGGACGTGGGGCAGAC as the reverse primer. The PCR product was digested with *Nco*I and *Bam*HI (cleavage sites highlighted above), gel purified, and ligated into *Nco*I- and *Bam*HI-digested pHIS8. Automated nucleotide sequencing (Salk Institute DNA sequencing facility) was used to verify the complete nucleotide sequences of all of the above-mentioned constructs.

Expression and Purification of RPTPα D2 and Src SH2. Constructs of pET-28a(+) RPTPα D2 and pHIS8 Src SH2 were transformed into *E. coli* strain BL21(DE3). Plasmid-containing *E. coli* cells were grown at 37 °C in Terrific broth containing 50 μg/mL kanamycin until A_{600} reached 1.0. The temperature of the cultures was reduced to 18 °C, and protein expression was induced with 0.5 mM isopropyl 1-thio-β-D-galactopyranoside. After growing for 5 h, cells were pelleted and resuspended in lysis buffer containing 50 mM Tris-HCl (pH 8.0), 500 mM NaCl, 20 mM imidazole (pH 8.0), 20 mM β-mercaptoethanol, 10% (v/v) glycerol, 1% (v/v) Tween-20, 1 mM benzamidine, and 1 mM PMSF. The cell suspensions were sonicated, and the supernatants were passed over a 2 mL Ni^{2+}−NTA column. The columns were washed with 5 bed volumes (10 mL) of lysis buffer and 5 bed volumes (10 mL) of lysis buffer without Tween-20, benzamidine, and PMSF. His-tagged proteins were eluted with 15 mL of lysis buffer without Tween-20, benzamidine, and PMSF, but with 250 mM imidazole (pH 8.0). The eluates were then dialyzed for 24 h at 4 °C against 50 mM Tris, 500 mM NaCl, and 20 mM β-mercaptoethanol in the presence of 10 μg of thrombin to cleave the His tags. Dialyzed and cleaved proteins were passed over Ni^{2+}−NTA resin and benzamidine-Sepharose to remove His tag-containing proteins and thrombin, respectively. Proteins were further purified by gel filtration on a Superdex-200 FPLC column equilibrated in 50 mM Tris (pH 8.0), 500 mM NaCl, and 1 mM DTT. The peak fractions were collected and dialyzed for 24 h at 4 °C against 50 mM Tris (pH 8.0), 100 mM NaCl, and 1 mM DTT. Proteins were then concentrated to 12 mg/mL for RPTPα D2 and 18 mg/mL for Src SH2, aliquoted, and stored at −80 °C.

Data Collection and Structure Determination. Crystals of RPTPα D2 were grown at 4 °C by vapor diffusion in hanging drops consisting of a 1:1 mixture of protein and crystallization buffer [15% (w/v) PEG8000, 0.1 M sodium succinate (pH 5.5), 1 mM DTT, and 0.25 M Li_2SO_4 ($P3_1$ form)]. Crystals grew to their maximal size within 48 h. Crystals of the Src SH2·D2 phosphopeptide complex (CDpYANFK) at a 1:1 molar ratio were grown at 4 °C by vapor diffusion in hanging drops consisting of a 1:1 mixture of protein and crystallization buffer [30% (w/v) PEG8000, 0.2 M sodium acetate, 0.1 M sodium cacodylate (pH 6.5), and 1 mM DTT]. These crystals also grew to their maximal size after 48 h. Diffraction data were obtained at the Stanford Synchrotron Radiation Laboratory (Palo Alto, CA) at beam lines 7-1 (RPTPα D2, $P3_1$ form) and 9-1 (Src SH2 + D2 peptide). Single crystals were mounted on a cryoloop, flash-frozen in a nitrogen stream at 105 K, and screened in-house using a MacScience DIP2030 imaging plate system and Cu Kα radiation produced by a rotating anode operated at 45 kV and 100 mA and equipped with double-focusing Pt/Ni-coated mirrors. Images were indexed and integrated using DENZO and the reflections merged with SCALEPACK (*26*).

The structure of RPTPα D2 was determined by molecular replacement using CNS (*27*) and RPTPα D1 as a search model (*5*). The Src SH2·D2 phosphopeptide complex was determined by molecular replacement using EPMR (*28*) and a Src SH2 structure as a search model (*29*). All protein models were refined using CNS (*27*). Electron density maps were inspected, and model building was performed in O (*30*). Water molecules identified in CNS were checked and retained if visible. Composite omit maps were calculated in CNS (*27*) and compared with the current models to rule out model bias and improve stereochemistry. Model quality was confirmed using PROCHECK (*31*). Atomic coordinates and structure factors for RPTPα D2 and the Src SH2·D2 phosphopeptide complex have been deposited in the Protein DataBank as entries 1P15 and 1P13, respectively.

Limited Proteolysis. RPTPα D1D2 (630 μg) was incubated on ice in the presence of 50 mM Tris-HCl (pH 8.0), 1 mM DTT, and 500 ng of trypsin for 0.15, 5, 10, 20, 40, 80, and 120 min or with 1 μg of chymotrypsin at 25 °C for 10, 20, 40, 80, 160, and 320 min and 16 h. Reactions (total volume of 70 μL) were quenched by addition of 40 μL of 1× SDS−PAGE sample buffer [25 mM Tris-HCl (pH 6.8), 20% (w/v) glycerol, 4% (w/v) SDS, bromophenol blue, and β-mercaptoethanol] to 5 μL of the proteolysis reaction mixture at the indicated times. Proteolytic fragments were separated by SDS−PAGE (15% acrylamide and 0.4% bisacrylamide), transferred to a polyvinylidene difluoride membrane (PVDF), and stained with Amido Black. Individual bands were excised by cutting and sequenced by Edman degradation.

Anisotropy Binding Experiments. N-Terminal rhodamine-labeled D2 peptide {6-[tetramethylrhodamine-5(6)-carboxamidohexanoic acid]-AFSDpYANFK} was resuspended in 50 mM Tris-HCl (pH 8.0), 150 mM NaCl, and 1 mM DTT to a concentration of 2 mM and stored at −80 °C. Fluorescence data were obtained on a PTI Alphascan spectrofluorimeter (Photon Technology Instruments, Santa Clara, CA). Dissociation equilibrium constants were determined by measuring the change in fluorescence anisotropy of a peptide at a constant concentration while varying the concentration of the Src SH2 domain as described previously (*32*).

RESULTS

Determination of the Structure of the D2 Domain. Murine RPTPα D2 tyrosine phosphatase domain (residues Ile512−Ser787) crystals were obtained within 48 h at 4 °C using 15% (w/v) PEG8000, 0.1 M sodium succinate (pH 5.5), 1 mM DTT, and 0.25 M Li_2SO_4. The structure was determined by molecular replacement using CNS (*27*) together with the published structure of RPTPα D1 as a search model (*5*). Two molecules of D2 were found per asymmetric unit, but they were not related by a 2-fold rotation axis. These polypeptide chains were built in O (*30*) and refined using CNS (*27*). The $P3_1$ crystal was twinned, but could be refined using CNS detwinning software to a resolution of 2.0 Å (Table 1).

Overall D2 Structure and Comparison with the Structure of the RPTPα D1 Domain. The D2 domain of RPTPα adopts a globular fold consisting of an eight-stranded twisted β-sheet

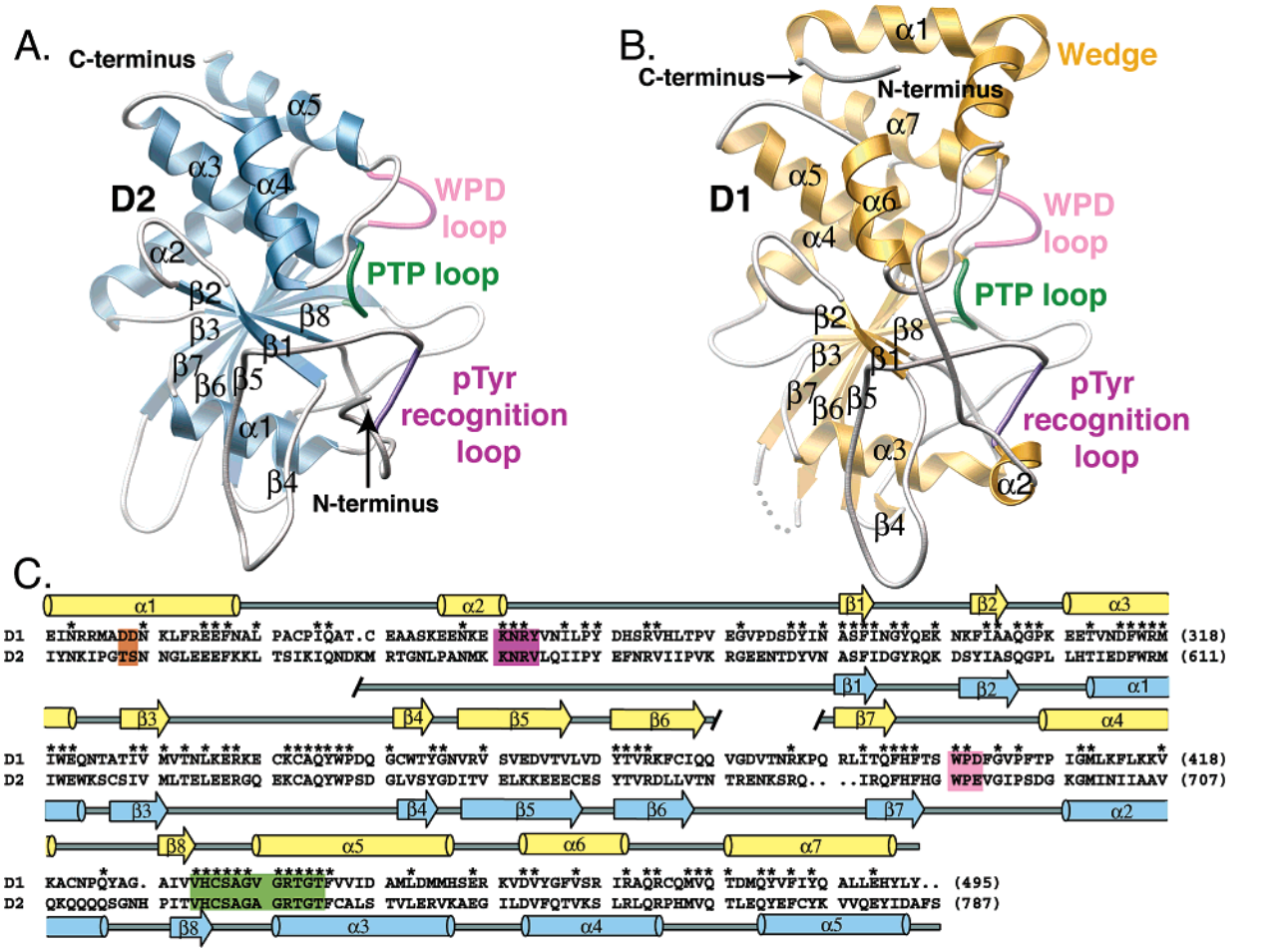

FIGURE 1: (A) Ribbon trace of the overall fold of the RPTPα D2 domain shown in blue. The N- and C-termini are labeled as are the α-helices and *β*-strands. The WPD loop is shown in pink; the phosphotyrosine phosphatase (PTP) binding loop is shown in green, and the pTyr recognition loop is shown in purple. Residues 512−540 (N-terminal region) were not visible in the electron density maps and, therefore, are not depicted in the models. (B) Ribbon trace of the RPTPα D1 domain shown in yellow. The N- and C-termini are labeled as well as the wedge motif; residues Val379−Pro387 were not visible in the electron density and are modeled as a dotted line. The WPD loop is shown in pink; the PTP loop is shown in green, and the pTyr recognition loop is shown in purple. (C) Sequence and secondary structure alignment of the D1 (gold) and D2 (blue) domains of RPTPα. The amino acids that encompass the WPD loop are shaded pink; the PTP loop is shown in green, and the pTyr recognition loop residues are shaded purple. Residues involved in wedge-mediated interactions in D1, namely, Asp227 and Asp228, are highlighted in orange. Conserved residues are marked with asterisks. The beginning of the D2 sequence is the start of the protein sequence that was crystallized. The first visible residue in the crystal structure of D2 is denoted with a black hatch mark. An unstructured loop in D1 linking *β*-strand 6 to *β*-strand 7 is represented by a set of hatch marks.

surrounded by four α-helices on one side and one α-helix on the other. Comparison of RPTPα's D2 domain (blue) with the D1 domain (gold) reveals a high degree of both sequence and structural identity; the rmsd between α-carbons is 1.04 Å as measured in O (Figure 1). The overall architecture of D2 is also similar to those of other known protein tyrosine phosphatase structures, including PTP1B (*33*), the RPTP*μ* D1 domain (*11*), and both the D1 and D2 domains of LAR (*12*). The most striking difference between RPTPα's D1 and D2 phosphatase domains is the absence of the helix−loop−helix wedge motif in the D2 domain (Figure 1A,B). A sequence alignment between the wedge motif of RPTPα D1 (α-helices 1 and 2) and the corresponding region in D2 reveals a level of amino acid identity of 22% compared to a value of 38% for the overall pairwise alignment of phosphatase domains (Figure 1C). Furthermore, two residues in the D1 wedge motif that participate in interactions across the dimer interface, Asp227 and Asp228, are Thr and Ser, respectively, in the corresponding region of D2 (*5*). Strikingly, the electron density for the residues that would encompass the region spanning the wedge motif in RPTPα's

Table 1: Crystallographic Data and Refinement Statistics for Human RPTPα D2 and the Complex of Avian Src's SH2 Domain with a Phosphopeptide Derived from the C-Terminal Region of RPTPα D2

	RPTPα D2	SH2·D2 peptide
maximum resolution (Å)	2.0	1.6
space group	$P3_1$	$P2_12_12_1$
unit cell dimensions (Å)	$a = b = 59.1$, $c = 152.7$	$a = 58.4$, $b = 58.8$, $c = 62.7$
twinning fraction	0.443	−
twinning operator	$h+k, -k, -l$	−
R_{sym}[a,b] (%)	4.1 (40.2)	5.7 (42.3)
no. of total observations	442014	234548
no. of unique reflections	40834	27413
completeness[a] (%)	96 (92)	98 (69)
I/σ[a]	30.9 (4.1)	20.6 (2.6)
R_{cryst}[c] (%)	20.7	20.1
R_{free}[d] (%)	25.3	24.7

[a] Numbers in parentheses are for the highest-resolution shell. [b] $R_{sym} = \sum|I_h - \langle I_h\rangle|/\sum\langle I_h\rangle$, where I_h is the average intensity over symmetry equivalent reflections. [c] $R_{cryst} = \sum|F_{obs} - F_{calc}|/\sum F_{obs}$, where summation is over the data used for refinement. [d] R_{free} has the same definition as R_{cryst}, but includes only 10% of data excluded from refinement.

D2 domain (Ile512−Lys540) is not visible, and thus, these residues are disordered.

Other structural motifs critical for protein tyrosine phosphatase activity are conserved between the D1 and D2 domains. The PTP loop (shown in green, Figure 1A,B), a conserved sequence motif [(I/V)HCXAGAGR(S/T)] found in all tyrosine phosphatases, is located at the base of the catalytic cleft between β-strand 8 and α-helix 5 (D1) or α-helix 3 (D2), and contains the active site cysteine required for catalysis. RPTPα D2 retains some catalytic activity, but it has a k_{cat} that is 1 order of magnitude lower and a K_m that is 5-fold higher for the substrate *p*-nitrophenol phosphate than those of the D1 domain. The D2 structure provides insights into why it has low catalytic activity. The conserved active site cysteine is present in D2, and its location is identical to that if the corresponding cysteine of D1 (*34*). A second conserved structural motif, the pTyr recognition loop, shown in purple, is composed of residues KNRY and is involved in substrate binding, specifically recognizing the phenyl ring of the pTyr residue and defining the depth of the pTyr recognition pocket. Although the position of the pTyr recognition loop is conserved between domains, the D2 sequence has a Val in place of the Tyr found in the KNRY motif (KNRV) (Figure 1C). A third critical and conserved region in tyrosine phosphatases is the WPD loop (shown in pink), which is involved in substrate binding. Like the pTyr recognition loop, the WPD loop location is conserved between D1 and D2 domains; however, the D2 domain contains the conservative substitution of a Glu instead of an Asp (WPE). Thus, the low activity of D2 is not due to major changes in three-dimensional structure, and the amino acid differences in the KNRY and WPD motifs must be responsible (see below).

RPTPα D2 Crystallizes as a Monomer. The crystal form of RPTPα D2 reveals a monomeric arrangement of the D2 domain. This is in sharp contrast to the two crystal forms of the D1 domain, both of which contain an identical dimeric arrangement of occluded monomers with the inhibitory wedge motif of one molecule inserted into the active site cavity of the other enzyme, resulting in a catalytically inactive dimer (*5*). A monomeric D2 domain was not entirely unexpected since the domain is a monomer as assessed by gel filtration chromatography (data not shown) and dynamic light scattering (A. Bilwes, unpublished observation). The lack of occluded D2 dimers in both crystal forms, however, does not preclude the ability of full-length RPTPα to form dimers *in vivo*. Recently gathered data have shown that the D2 domain may not be required for RPTPα dimer formation. Specifically, Tertoolen et al. observed transmembrane domain-mediated RPTPα dimer formation in cells by fluorescence resonance energy transfer. The authors conclude that the wedge motif of D1 may only serve to stabilize the dimeric arrangement but is not required for dimer formation (*7*). However, other studies suggest that the D2 domain, while not sufficient for dimerization, may contribute to RPTPα dimer formation and stabilization. RPTPα with its D2 domain deleted decreases, but does not abolish, the amount of dimer formation *in vivo*, indicating that D2 may play a stabilizing role but most likely does not provide the predominant energetic driving force for dimerization (*8*). It is clear from the structures presented here that the D2 domain alone is not sufficient for formation of stable dimers *in vitro*. However, *in vivo*, D2 dimers have been isolated by immunoprecipitation after peroxide treatment, indicating that D2 dimers may form within certain cellular environments (*15*). On the basis of chemical cross-linking studies, we have previously suggested that RPTPα dimerization is mediated by a zipper-like effect, in which no single domain is by itself capable of driving stable dimer formation but rather a set of weaker interactions spread over the length of RPTPα support dimerization (*8*). Repeated attempts to obtain RPTPα D1D2 crystals for investigation of its oligomeric state have been unsuccessful. However, the D1D2 protein is monomeric as measured by gel filtration chromatography (data not shown). Thus, if this construct does form dimers *in vitro*, these oligomers may be transient and low-affinity, perhaps requiring the transmembrane and/or extracellular domain for stabilization.

Catalytic Alignment. While both D1 and D2 domains share a common active site architecture, key residues required for maximal catalytic activity are absent in the D2 domain. Figure 2A presents an overall structure overlay of the D1 domain (shown in gold) and the D2 domain (shown in blue) with the active site region denoted by a black box. The "catalytic" cysteine of D2, Cys723, is located at the back of the active site cavity in the PTP loop residing in a position identical to that of the catalytic cysteine of D1, namely, Cys433. RPTPα D2 contains Glu690 at the position normally occupied by an Asp residue in functional tyrosine phosphatase domains. Universally, this Asp residue is responsible for acting as a general acid−base catalyst during the dephosphorylation reaction of active tyrosine phosphatase domains (reviewed in ref *3*). Glu690 is located on a loop between β-strand 7 and α-helix 2 at the position identical to that of the corresponding Asp401 from D1 but extending further into the catalytic cavity (Figure 2B). D2's pTyr recognition loop contains Val555 in place of Tyr262 in the D1 domain. Tyr262 is a highly conserved residue among functional tyrosine phosphatase domains and is important in forming a hydrophobic and aromatic surface upon which the phenyl ring of the pTyr residue stacks.

The low activity of D2 *in vitro* is the result of the substitution of Asp and Tyr for Glu690 in the WPD loop and Val555 in the pTyr recognition loop, respectively. A D2 double mutant (E690D/V555Y) displays pTyr phosphatase activity against the substrate *p*-nitrophenyl phosphate with kinetic parameters approaching the values measured for the D1 domain with a K_m 2 times larger and a k_{cat} that is 1.3 times larger than those for D1 (*34*). By comparison, wild-type D2 has a K_m value that is 5 times larger and k_{cat} value that is 10 times smaller than those of D1 (*34*). However, it was unclear whether the significant increase in catalytic activity was a result of changing the identity of the two amino acids or if mutations allowed proper alignment of these key residues of the D2 domain during substrate turnover. The D2 structure presented here confirms that the identity of these crucial residues and not their three-dimensional location is responsible for the minimal D2 catalytic activity. Since these substitutions at the WPD and pTyr recognition loops are highly conserved among D2 domains, significant pTyr phosphatase activity must not be crucial to the function of the D2 domain.

The D2 N-Terminal Polypeptide Is Disordered. Electron density for the D2 domain begins at Met541, 29 residues

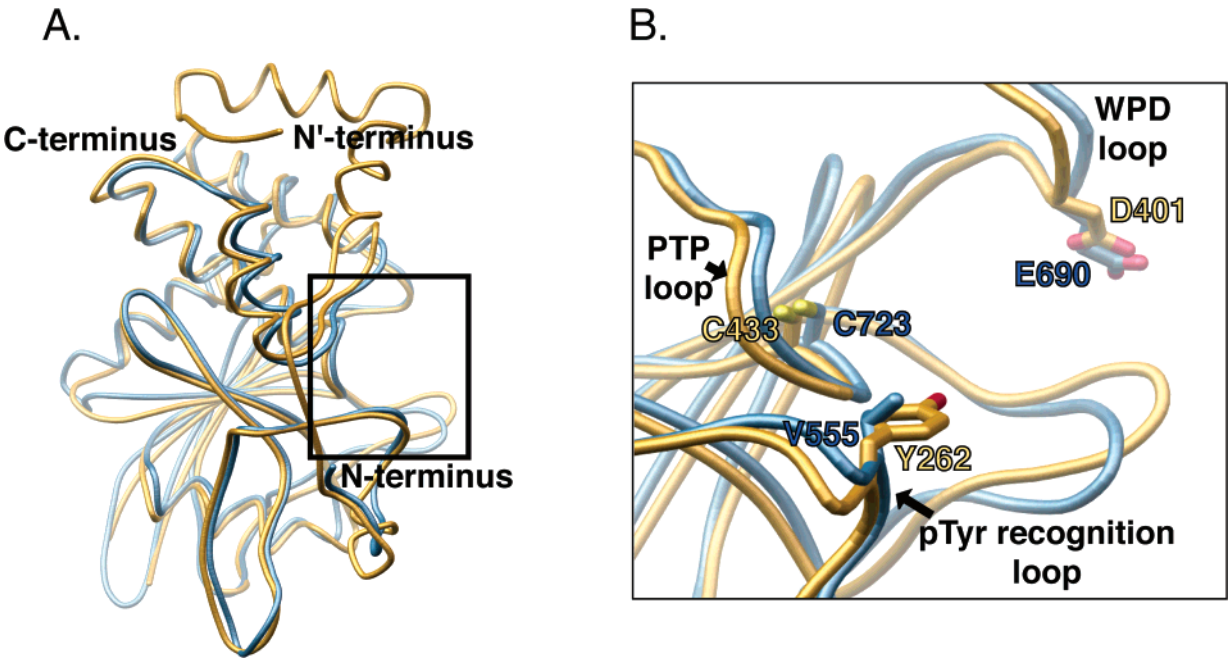

FIGURE 2: Comparison of the RPTPα D1 and D2 active site regions. (A) Overlay of the crystal structure of the D1 domain (gold) with the D2 domain (blue). N′-Terminus and N-terminus highlight the start of the D1 and D2 structures, respectively. The active site region is surrounded by a black box. (B) Magnified active site cleft of D1 (gold) and D2 (blue). The PTP, WPD, and pTyr recognition loops are labeled. Highlighted residues include the catalytic cysteines (Cys433 in D1 and Cys723 in D2), the putative general acids/bases (Asp401 in D1 and Glu690 in D2), and the hydrophobic pTyr clamps (Tyr262 in D1 and Val555 in D2).

after the start of the protein sequence used for crystallization. To rule out the possibility of proteolysis and loss of the first 29 residues of the crystallized construct during protein purification or crystallization, the D2 protein both following purification and resolubilized from the crystalline state was subjected to N-terminal sequencing by Edman degradation. The sequence results confirm that the N-terminal residue of D2 from both the protein preparation and crystal is Ile512, eliminating the possibility of proteolysis occurring during purification or crystallization (data not shown). The absence of electron density for the 29 amino-terminal residues implies that this region is highly flexible.

To identify the flexible regions within the D2 structure, *B*-factor values for the protein backbone were investigated. Figure 3 shows the backbone α-carbon trace color-coded for *B*-factor values with the red regions displaying high *B*-factors (maximum of 75 Å^2), the blue regions containing low *B*-factors (minimum of 19 Å^2), and intermediate values encoded by a gradient of colors from blue to red. There are three regions of high *B*-factors in the D2 domain. The first region encompasses the end of α-helix 2 (denoted with one asterisk). Not surprisingly, a second area of flexibility in the D2 domain resides in the loop linking *β*-strands 6 and 7 (denoted with two asterisks). The analogous loop in the D1 domain structure is missing from the electron density (*5*). The final region displaying high *B*-factors includes the N-terminal loop (Figure 3, denoted with three asterisks).

To further evaluate the flexibility at the N-terminus of D2, we embarked on a limited proteolysis study of the intracellular domain (D1D2) of RPTPα. Specifically, purified RPTPα D1D2 protein, Lys208−Ser787 (630 *μ*g), was incubated with trypsin (500 ng) on ice for up to 2 h or chymotrypsin (1 *μ*g) at 25 °C for up to 16 h. Proteolytic fragments were separated by SDS−PAGE and transferred to a PVDF membrane, and all major bands were excised

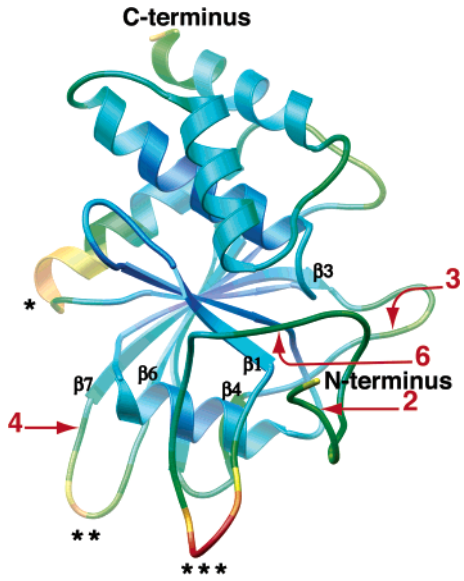

FIGURE 3: Visual representation of flexible regions within the D2 domain. Ribbon diagram of the RPTPα D2 domain shaded by *B*-factor values. Relatively high *B*-factors (maximum of 75 Å^2) are shown in red; low *B*-factors (minimum of 19 Å^2) are colored blue, and intermediate values are coded by a gradient of colors from blue to red. The three regions exhibiting the highest *B*-factors are denoted with asterisks: one asterisk, located at the end of α-helix 2; two asterisks, located between *β*-strands 6 and 7; and three asterisks, located in the N-terminal loop region. Both N- and C-termini are labeled. Red arrows and the associated numbers denote proteolytically sensitive sites as diagrammed and discussed in Figure 4. Secondary structural elements that encompass each of these designated sites (2, 3, 4, and 6) are shown.

and subjected to N-terminal sequencing by Edman degradation (Figure 4A,B). The resulting N-terminal proteolytic cut sites are denoted by red arrows above the D1D2 primary sequence with the crystallographically determined secondary structure shown. Bands not denoted with an arrow contained

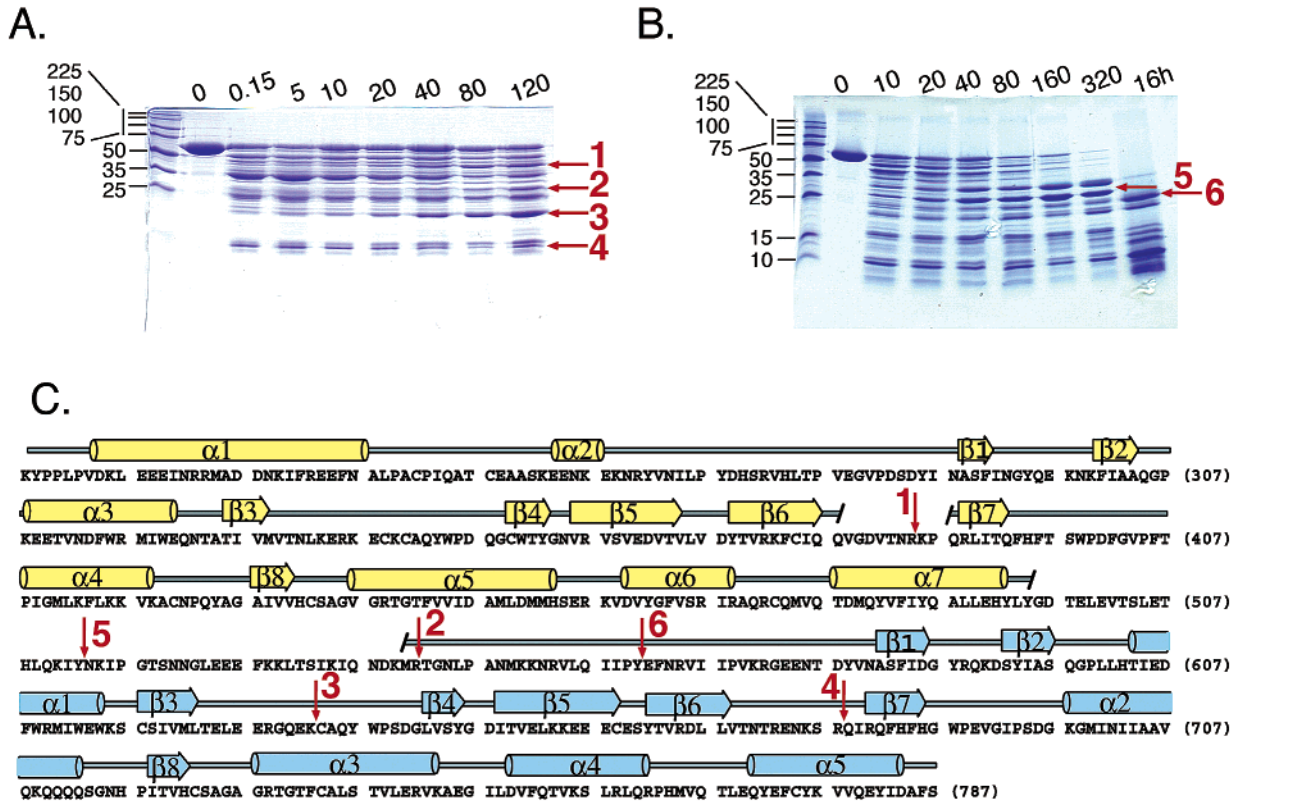

FIGURE 4: Limited proteolysis of the RPTPα D1D2 intracellular domain protein. (A) Trypsin digest of RPTPα D1D2 separated by SDS−PAGE (15% acrylamide/0.4% bisacrylamide) and stained with Coomassie Blue. The times before quenching are shown in minutes above each lane. Molecular weight standards are shown in lane 1, and uncut RPTPα D1D2 is in lane 2. Bands excised for N-terminal sequencing are denoted with a red arrow and numbered. Unlabeled bands contained an intact N-terminus. (B) Chymotrypsin digest of RPTPα D1D2 separated by SDS−PAGE (15% acrylamide/0.4% bisacrylamide) and stained with Coomassie Blue. Time periods prior to quenching are given in minutes. Molecular weight standards are shown in lane 1, and uncut RPTPα D1D2 is in lane 2. Protein bands excised for N-terminal sequencing are denoted with a red arrow and numbered. Unlabeled bands contained an intact N-terminus. (C) Sequence and secondary structure depiction of RPTPα with the D1 domain shown in gold and the D2 domain in blue. Red arrows highlight cleavage sites with the numbers corresponding to the numbered bands shown in panels A and B.

an intact N-terminus. Presumably, these bands correspond to the N-terminal halves of the molecules cleaved to generate fragments with an internal N-terminus. A tryptic cleavage site occurs following Arg385, which is located in the loop spanning β-strands 6 and 7 in the D1 domain (arrow 1). This same region is absent from the electron density maps in both D1 domain crystal structures (*5*). The corresponding peptide backbone in D2 is also susceptible to proteolytic digestion with trypsin with cleavage occurring after Arg678 (arrow 4). Within the folded D2 domain, a second tryptic cleavage site, Lys633 (arrow 3), resides on an exposed loop near the active site cavity in D2. Importantly, three additional and distinct proteolytically labile positions are peppered throughout the linker polypeptide segment joining D1 to D2 (residues Ser504−Gln537) and along the N-terminal segment of RPTPα's D2 domain. Notably, cleavage occurs following Tyr513, Arg542, and Tyr561 (highlighted by arrows 5, 2, and 6, respectively, in Figure 4C). Arg542 (arrow 2) sits one residue removed from where the electron density for D2 begins. The proteolysis and structural data support the presence of interdomain flexibility between D1 and D2 domains in RPTPα. The proteolytically labile regions of RPTPα also correlate nicely with the *B*-factor values for the D1 and D2 crystal structures, with regions of high *B*-factors exhibiting proteolytic sensitivity (Figure 3B). Moreover, the difficulty associated with obtaining crystalline D1D2 protein may be a further indication of a great deal of flexibility within the region between D1 and D2.

D2 N-Terminal Flexibility May Be Common among RPTPs. The only published example of a crystal structure containing both D1 and D2 phosphatase domains of an RPTP is the structure of LAR (shown in Figure 5A). In this structure, the two phosphatase domains are connected by a conserved four-residue linker that is N-terminal to the spacer region in an orientation that precludes wedge-mediated dimerization described for RPTPα (*12*). Comparison of the D2 domain from RPTPα (shown in blue) and from LAR (shown in orange) shows the large structural conservation shared between family members (Figure 5B). However, the LAR D2 domain contains a helix−loop−helix motif in the D2 spacer region reminiscent of the wedge motif found in the D1 domain, but the corresponding motif is not present in the D2 domain of RPTPα. A schematic of the RPTPα intracellular domain organization is shown in Figure 5C. The RPTPα D2 domain protein used for crystallization contains the proper number of residues required to form the helix−loop−helix motif seen in the LAR D2 domain (28 residues), but these residues are not ordered in the described RPTPα D2 crystal form. The level of amino acid sequence conservation of these 28 residues between LAR and RPTPα is relatively high (38% identical). Perhaps crystallization of the LAR D1 and D2 domains in tandem allows formation and

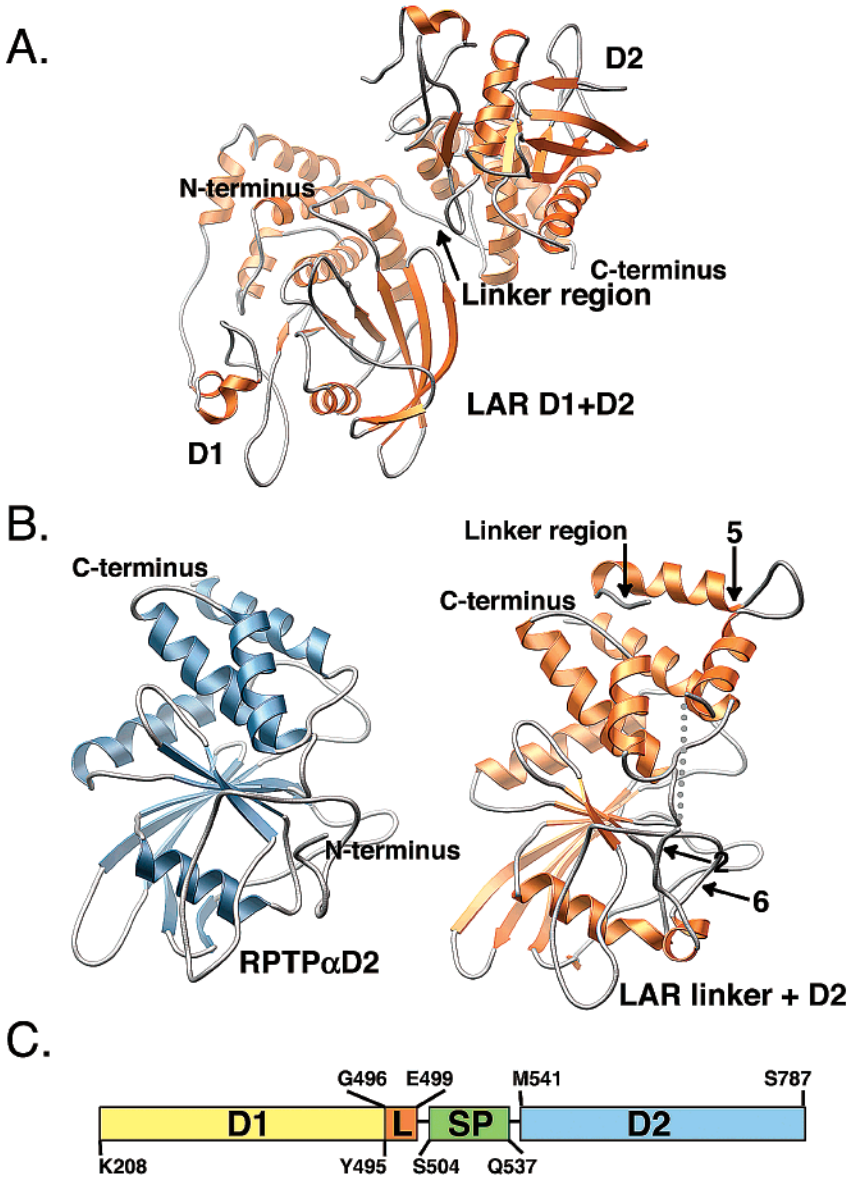

FIGURE 5: (A) Overall structure of the intracellular domain (D1 and D2) of LAR (*12*). Both D1 and D2 catalytic domains are labeled as are the N- and C-termini; an arrow denotes the four-residue linker region seen in LAR. (B) The D2 domain of RPTPα is shown in blue, and the D2 domain of LAR is shown in orange. The N- and C-termini are labeled, as is the linker region in the LAR D2 structure. An area of missing electron density in the LAR structure is denoted with a dotted line. The corresponding regions that are susceptible to proteolysis are mapped on the analogous regions in the LAR structure and highlighted with arrows and the numbers that correspond to those used in Figure 4. (C) Schematic of RPTPα intracellular domain structure. The D1 domain is shown in gold, the linker region (L) orange, the spacer region (SP) green, and the D2 domain blue. The numbering is for RPTPα.

stabilization of the helix−loop−helix motif found in the D2 domain. In fact, close inspection of the crystal packing arrangement of the LAR crystal structure reveals that the helix−loop−helix region in the D2 domain is in close contact with this same motif in a symmetry-related D2 domain. The determination of additional RPTP crystal structures and/or the structure of D1D2 RPTPα may resolve whether the ability to form a helix−loop−helix motif is common in all D2 domains or unique to the LAR RPTP.

The LAR D2 domain contains a segment comprised of four residues located on the C-terminal side of the helix−loop−helix motif within the spacer and the N-terminal portion of the D2 phosphatase domain that is not visible in the electron density maps (shown as a dotted line in Figure 5B) (*12*). The beginning of the visible electron density C-terminal to the disordered region occurs at a position analogous to the position where the electron density in the RPTPα D2 domain becomes visible, indicating that this region is flexible in both the RPTPα and LAR crystals. Mapping the RPTPα proteolytic sites on the analogous positions in the LAR D2 structure reveals that the proteolytically labile regions are within the helix−loop−helix motif (spacer region), as well as the N-terminal portion of the D2 domain (Figure 5B). The mapping of the flexible regions of RPTPα onto LAR suggests that wedge-mediated dimer formation in LAR may be possible assuming that there is rotational freedom allowed within the disordered region of LAR D2.

A dynamic model that incorporates all of the static RPTP structures determined to date is one in which the D1 and D2 domains are connected by a highly flexible linker−D2 N-terminal region. Consistent with this model, a number of

papers have reported that the D1 domains of some RPTPs can interact with various D2 domains in an interdomain fashion. Specifically, Blanchetot et al. have demonstrated an intramolecular interaction between the spacer region (Ser504−Gln537) and the C-terminal portion of RPTPα upon treatment with H_2O_2 (*15*). Furthermore, phosphorylation of Ser180/204 in the juxtamembrane region, N-terminal to D1, affects the ability of c-Src to interact with a pTyr residue located near the C-terminus of RPTPα, suggesting that the juxtamembrane region contacts or abuts the C-terminal portion of RPTPα (*23*). Importantly, however, it was not shown unequivocally that the juxtamembrane−C-terminus interaction occurs in an intramolecular fashion. In the case of another RPTP family member, CD45, an intramolecular interaction between the D1 and D2 domains was also reported (*13*). Keeping in mind that RPTPs are restricted to two-dimensional diffusion as a result of their integration into the membrane bilayer, we find it difficult to imagine how these domains might interact intra- or intermolecularly if a rigid linker tethers D1 to D2. The crystallographic and proteolytic data above support the importance of flexibility between D1 and D2 domains that may be critical for intramolecular D1−D2 associations.

Role for D2 in Mediating Substrate Binding in Vivo through Its C-Terminal Polypeptide. While a definitive functional role for D2 during substrate turnover remains unclear, some have proposed that D2 domains serve as substrate recruitment modules, thus increasing the local substrate concentration near the more active D1 domain (reviewed in ref *35*). Specifically, the D2 domain of CD45 is required to recruit its substrate TCR-ζ since replacement of CD45's D2 domain with the D2 domain of LAR results in a loss of D1−TCR-ζ association and subsequent dephosphorylation of TCR-ζ (*20*). In a similar fashion, LAR recognizes one of its substrates, the insulin receptor, via its D2 domain (*36*). The C-terminal tail of RPTPα's D2 domain contains a pTyr residue (Y789) that is phosphorylated to a stoichiometry of approximately 20% *in vivo* in unstimulated cells (*21*). This phosphorylation site is known to be recognized by the SH2 domain of Grb2 and more recently has been shown to bind the SH2 domain of the RPTPα substrate c-Src (*22*, *37*). SH2 domain-mediated binding of c-Src to RPTPα is required to unravel c-Src's inhibitory restraints, allowing the inhibitory phosphorylation site on c-Src's C-terminus to be dephosphorylated by RPTPα which culminates in c-Src activation (*22*, *23*).

For a closer look at the binding of Src's SH2 domain to the C-terminal phosphorylation site of D2, the SH2 domain of chicken c-Src was crystallized in the presence of an equal molar ratio of a seven-residue pTyr-containing peptide in which the six C-terminal residues correspond to the six C-terminal residues of RPTPα (CDpYANFK). This crystal structure was determined by molecular replacement using the published structure of the Src SH2 domain complexed with ace-malonyl Tyr-Glu-(*N*,*N*-dipentylamine) and refined to a resolution of 1.8 Å (Table 1) (*29*). The overall topology of the SH2 domain is very similar to that described for the previously determined Src SH2 structure complexed with the peptide pYEEI with an rmsd between α-carbons of 0.98 Å (*38*, *39*). Briefly, the SH2 domain is comprised of a seven-stranded β-sheet core with one α-helix on each side of the core β-sheet. D2's C-terminus (shown in purple) binds to the SH2 domain (shown in green) in an extended conformation with the pTyr residue bound in a polar lined pocket and the +3 Phe residue bound in a second pocket lined with hydrophobic residues (Figure 6A). An overlay of the current structure (shown in green) with the previous Src SH2 domain−pYEEI peptide structure (shown in gold) reveals an overall conservation of fold and peptide recognition. One striking exception is the phosphate binding loop between the second and third β-strands, which in the current structure is positioned 8.5 Å, at its farthest point, from the corresponding loop in the previously determined SH2 structure (Figure 6B). This loop forms one face of the pTyr-binding pocket and contains residues Ser190, Glu191, and Thr192 that are important for recognition of the phosphate moiety of the pTyr residue. In the structure of Waksman et al. (*38*, *39*), the hydroxyl groups of Ser190, Glu191, and Thr192 are positioned 2.8, 5.0, and 2.7 Å, respectively, from the phosphate group of the pTyr residue. However, in our structure, these residues are too far away to make contacts with the phosphate group, namely, 7.2, 9.4, and 10.3 Å away for Ser190, Glu191, and Thr192, respectively (Figure 6C,D). It is unclear why

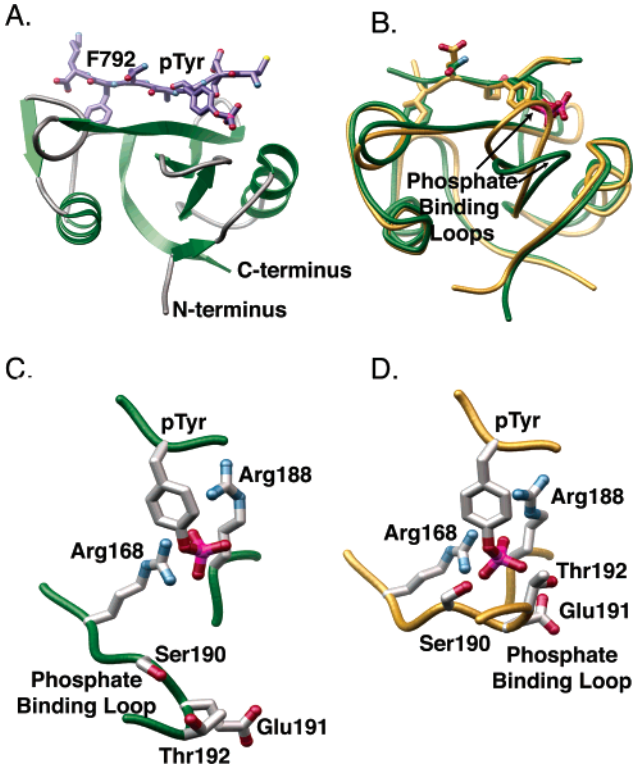

FIGURE 6: (A) Structure of the SH2 domain of avian Src (shown in green) bound to a pTyr-containing peptide derived from the C-terminal region of the RPTPα D2 domain (shown in purple). The N- and C-termini are labeled along with the pTyr residue and the +3 residue (relative to pTyr), Phe792. (B) Overlay of the current Src SH2·peptide complex bound to the peptide, CDpYANFK (shown in green), and a previously reported Src SH2 domain bound to pYEEI (*38*) shown in gold with the phosphate binding loops labeled. (C) Close-up view of the pTyr-binding pocket of the current Src SH2 domain shown in green. Arg168 and Arg188, critical residues for pTyr binding, are shown, as well as Ser190, Glu191, and Thr192, which form part of the phosphate binding loop. (D) Close-up view of the pTyr-binding pocket of a previously reported Src SH2 domain·peptide complex shown in gold (*38*). Arg168, Arg188, and residues involved in pTyr binding are shown. All crystallographic structure models presented here were rendered with MOLSCRIPT (*43*) and POV-Ray (*44*).

in this case the loop is positioned so far from the pTyr residue.

On the other face of the pTyr-binding pocket are two residues highly conserved in SH2 domains and extremely important in pTyr binding, Arg168 and Arg188 located on α-helix 1 and β-strand 1, respectively. The position of these residues is identical to that in previous SH2 structures. Arg168 is 2.9 Å and Arg188 2.8 Å from the pTyr phosphate moiety. A second pocket lined with hydrophobic residues Tyr215, Ile227, Tyr243, and Leu250 provides a cavity that nicely accommodates the +3 residue, Phe792, on the D2 C-terminal segment. Thus, the pTyr and +3 Phe residues from the D2 peptide fit like a plug into a two-pronged socket previously described for other Src SH2 domain structures (*39*).

The affinity of the D2 peptide for Src SH2 was measured by fluorescence anisotropy using a rhodamine-labeled phosphopeptide similar to the peptide sequence used for crystal structure analysis (AFSDpYANFK). The C-terminus of D2 binds the SH2 domain with an affinity of 4.0 ± 0.9 μM (data not shown), a value similar to those obtained previously for similar peptides, but still 1 order of magnitude weaker than the affinity for the optimal peptide sequence pYEEI (0.27 μM) measured previously (*40*). The affinity of the Src SH2 domain for the C-terminal portion of RPTPα D2 is lower than for the optimal peptide sequence, and our crystal structure reveals suboptimal peptide binding contacts. However, co-immunoprecipitation studies confirm a SH2 domain−RPTPα C-terminal interaction *in vivo* (*22*). Since accurate regulation of c-Src activity is critical for proper cellular signaling, high-affinity Src SH2 binding to RPTPα would be undesirable. RPTPα activation of c-Src is necessary only upon specific cellular signals, not constitutively. Therefore, a weak association ensures that c-Src activation occurs only when the proper cellular conditions are met. These conditions may include RPTPα Ser180/204 phosphorylation or the absence of inhibitory Grb2 sequestration and masking of the RPTPα C-terminus.

More recently, Zheng et al. have examined the ability of RPTPα to recognize the SH2 domain of Src versus the SH2 domain of Grb2 *in vivo*. They have shown that the majority of RPTPα is complexed with Grb2 under resting conditions. However, upon cellular stimulation, RPTPα undergoes protein kinase C-mediated serine phosphorylation at its juxtamembrane region (Ser180 and/or Ser204) coincident with release of Grb2 and binding of Src SH2 (*23*, *24*). The authors hypothesize that the Ser180/204 phosphorylation sites interact with the C-terminal pTyr region, allowing the C-terminus to adopt an extended conformation preferred by the SH2 domain of Src. However, direct evidence for this model has not been established. The displacement of Grb2 by protein kinase C-mediated phosphorylation and Src's SH2 domain allows RPTPα-mediated dephosphorylation of c-Src's inhibitory phosphorylation (Tyr527), resulting in c-Src activation (*23*). RPTPα has also been shown to bind and dephosphorylate the Src family member Fyn, indicating that the mechanism of c-Src activation mediated by RPTPα may be exploited by other Src family protein tyrosine kinases (*41*). In addition to RPTPα, RPTPε shares an identical consensus binding motif for Src family SH2 domains at its C-terminus and is able to complex the SH2 domain of Grb2 at RPTPε's analogous phosphorylation site, Tyr638 (*42*). Perhaps, the D2 domain of RPTPε also regulates c-Src or Src family members through a conserved mechanism involving displacement of Grb2 binding as has been hypothesized for RPTPα.

DISCUSSION

In this study, we show that the D2 tyrosine phosphatase domain of RPTPα alone is not sufficient for dimer formation, in contrast to what was previously observed for RPTPα D1. The D2 domain structures also differ from D1 in that they do not contain the helix−loop−helix inhibitory wedge motif. In contrast, the D2 N-terminal region, which corresponds to the helix−loop−helix region, is not visible in the electron density maps for D2 crystals. Proteolysis sensitivity studies confirm that the D2 N-terminal region is highly flexible, which may be functionally important for allowing intermolecular interactions with the D1 domains of various RPTP family members or substrate molecules. Flexibility would also be critical for facilitation of intramolecular interactions between the D2 domain's C-terminal region and the Ser180/204 phosphorylation sites present in RPTPα's juxtamembrane region as proposed by Zheng et al. (*23*).

The Src SH2 domain·D2 phosphopeptide complex structure reveals that the peptide adopts an extended conformation when bound to Src's SH2 domain. Furthermore, the pTyr and +3 Phe of the D2 peptide sit in each of two cavities located on the surface of the SH2 domain in a previously termed two-pronged socket model. One striking difference from previous Src SH2−peptide complex structures is the position of the phosphate binding loop that is approximately 10 Å, at the farthest point, from the pTyr phosphate moiety. The Src SH2−D2 peptide structure is consistent with affinity measurements showing suboptimal binding of the D2 C-terminus for the Src SH2 domain. Suboptimal Src SH2 binding may be critical to ensuring RPTPα activation of Src occurs in a highly regulated fashion.

ACKNOWLEDGMENT

We thank members of the Noel lab, the staff of the Stanford Synchrotron Radiation Laboratory (SSRL) for assistance during data collection on beam lines 9-1, 9-2, and 7-1, M. Verdecia for guidance with the fluorescence measurements, and C. Parks for the N-terminal sequencing.

REFERENCES

1. Petrone, A., and Sap, J. (2000) *J. Cell Sci. 133*, 2345−2354.
2. den Hertog, J., Blanchetot, C., Buist, A., Overvoorde, J., Van der Sar, A., and Tertoolen, L. G. J. (1999) *Int. J. Dev. Biol. 43*, 723−733.
3. Barford, D., Das, A. K., and Egloff, M. P. (1998) *Annu. Rev. Biophys. Biolmol. Struct. 27*, 133−164.
4. Tonks, N. K., and Neel, B. G. (2001) *Curr. Opin. Cell Biol. 13*, 182−195.
5. Bilwes, A. M., den Hertog, J., Hunter, T., and Noel, J. P. (1996) *Nature 382*, 555−559.
6. Jiang, G., den Hertog, J., Su, J., Noel, J., Sap, J., and Hunter, T. (1999) *Nature 401*, 606−610.
7. Tertoolen, L. G. J., Blanchetot, C., Jiang, G., Overvoorde, J., Gadella, T. W. J., Hunter, T., and den Hertog, J. (2001) *BMC Cell Biol. 2*, 8.
8. Jiang, G., den Hertog, J., and Hunter, T. (2000) *Mol. Cell. Biol. 20*, 5917−5929.
9. Majeti, R., Bilwes, A. M., Noel, J. P., Hunter, T., and Weiss, A. (1998) *Science 279*, 88−91.

10. Majeti, R., Xu, Z., Parslow, T. G., Olsen, J. L., Daikh, D. I., Killeen, N., and Weiss, A. (2000) *Cell 103*, 1059−1070.
11. Hoffmann, K. M. V., Tonks, N. K., and Barford, D. (1997) *J. Biol. Chem. 272*, 27505−27508.
12. Nam, H. J., Poy, F., Krueger, N. X., Saito, H., and Frederick, C. A. (1999) *Cell 97*, 449−457.
13. Felberg, J., and Johnson, P. (1998) *J. Biol. Chem. 273*, 17839−17845.
14. Feiken, E., van Etten, I., Gebbink, M. F. B. G., Moolenaar, W. H., and Zondag, G. C. M. (2000) *J. Biol. Chem. 275*, 15350−15356.
15. Blanchetot, C., Tertoolen, L. G. J., and den Hertog, J. (2002) *EMBO J. 21*, 493−503.
16. van der Wijk, T., Blanchetot, C., Overvoorde, J., and den Hertog, J. (2003) *J. Biol. Chem. 278*, 13968−13974.
17. Wallace, M. J., Fladd, C., Batt, J., and Rotin D. (1998) *Mol. Cell. Biol. 18*, 2608−2616.
18. Blanchetot, C., and den Hertog, J. (2000) *J. Biol. Chem. 275*, 12446−12452.
19. Blanchetot, C., Tertoolen, L. G., Overvoorde, L. G., and den Hertog, J. (2002) *J. Biol. Chem. 277*, 47263−47269.
20. Kashio, N., Matsumoto, W., Parker, S., and Rothstein, D. M. (1998) *J. Biol. Chem. 273*, 33856−33863.
21. den Hertog, J., Tracy, S., and Hunter, T. (1994) *EMBO J. 13*, 3020−3032.
22. Zheng, X. M., Resnick, R. J., and Shalloway, D. (2000) *EMBO J. 19*, 964−978.
23. Zheng, X. M., Resnick, R. J., and Shalloway, D. (2002) *J. Biol. Chem. 277*, 21922−21929.
24. Tracy, S., van der Geer, P., and Hunter, T. (1995) *J. Biol. Chem. 270*, 10587−10594.
25. Jez, J. M., Ferrer, J. L., Bowman, M. E., Dixon, R. A., and Noel, J. P. (2000) *Biochemistry 39*, 890−902.
26. Otwinowski, Z., and Minor, W. (1997) *Methods Enzymol. 276*, 307−326.
27. Brunger, A. T., et al. (1998) *Acta Crystallogr. D54*, 905−921.
28. Kissinger, C. R., Gehlhaar, D. K., and Fogel, D. B. (1999) *Acta Crystallogr. D55*, 484−491.
29. Charifson, P. S., Shewchuk, L. M., Rocque, W., Hummel, C. W., Jordan, S. R., Mohr, C., Pacofsky, G. J., Peel, M. R., Rodriguez, M., Sternbach, D. D., and Consler, T. G. (1997) *Biochemistry 36*, 6283−6293.
30. Jones, T. A., Zou, J. Y., Cowan, S. W., and Kjeldgaard (1993) *Acta Crystallogr. D49*, 148−157.
31. Laskowski, R. A., MacArthur, M. W., Moss, D. S., and Thornton, J. M. (1993) *J. Appl. Crystallogr. 26*, 283−291.
32. Vinson, V. K., De La Cruz, E. M., Higgs, H. N., and Pollard, T. D. (1998) *Biochemistry 37*, 10871−10880.
33. Barford, D., Flint, A. J., and Tonks, N. K. (1994) *Science 263*, 1397−1404.
34. Buist, A., Zhang, Y. L., Keng, Y. F., Wu, L., Zhang, Z. Y., and den Hertog, J. (1999) *Biochemistry 38*, 914−922.
35. Majeti, R., and Weiss, A. (2001) *Chem. Rev. 101*, 2441−2448.
36. Tsujikawa, K., Kawakami, N., Uchino, Y., Ichijo, T., Furukawa, T., Saito, H., and Yamamoto, H. (2001) *Mol. Endocrin. 15*, 271−280.
37. Tolendano-Katchalski, H., and Elson, A. (1999) *Oncogene 18*, 5024−5031.
38. Waksman, G., Kominos, D., Robertson, S. C., Pant, N., Baltimore, D., Birge, R. B., Cowburn, D., Hanafusa, H., Mayer, B. J., Overduin, M., Resh, M. D., Rios, C. B., Silverman, L., and Kuriyan, J. (1992) *Nature 358*, 646−653.
39. Waksman, G., Shoelson, S. E., Pant, N., Cowburn, D., and Kuriyan, J. (1993) *Cell 72*, 779−790.
40. Lubman, O., and Waksman, G. (2002) *J. Mol. Biol. 316*, 291−304.
41. Bhandari, V., Lim, K. L., and Pallen, C. J. (1998) *J. Biol. Chem. 273*, 8691−8698.
42. Katchalski, H. T., and Elson, A. (1999) *Oncogene 18*, 5024−5031.
43. Kraulis, P. J. (1991) *J. Appl. Crystallogr. 24*, 946−950.
44. POV-Team (1997) *POV-Ray: Persistence of vision ray-tracer*.

BI0340503